Journal of Power Sources 195 (2010) 8185–8188

Contents lists available at ScienceDirect

Journal of Power Sources

journal homepage: www.elsevier.com/locate/jpowsour

Short communication

A novel design of anode-supported solid oxide fuel cells with Y_2O_3-doped Bi_2O_3, $LaGaO_3$ and La-doped CeO_2 trilayer electrolyte

Weimin Guo [a,b], Jiang Liu [a,*]

[a] School of Chemistry and Engineering, South China University of Technology, The Key Laboratory of Enhanced Heat Transfer and Energy Conservation, Ministry of Education, Guangzhou 510640, PR China
[b] Department of Biological and Chemical Engineering, Guangxi University of Technology, Liuzhou 545006, PR China

ARTICLE INFO

Article history:
Received 10 June 2010
Received in revised form 13 July 2010
Accepted 13 July 2010
Available online 22 July 2010

Keywords:
Solid oxide fuel cells
Yttria-doped bismuth oxide
Strontium- and magnesium-doped lanthanum gallate
Trilayered composite electrolyte film
Comparison
Improvement

ABSTRACT

Anode-supported solid oxide fuel cells (SOFCs) with a trilayered yttria-doped bismuth oxide (YDB), strontium- and magnesium-doped lanthanum gallate (LSGM) and lanthanum-doped ceria (LDC) composite electrolyte film are developed. The cell with a YDB (18 μm)/LSGM (19 μm)/LDC (13 μm) composite electrolyte film (designated as cell-A) shows the open-circuit voltages (OCVs) slightly higher than that of a cell with an LSGM (31 μm)/LDC (17 μm) electrolyte film (designated as cell-B) in the operating temperature range of 500–700 °C. The cell-A using Ag-YDB composition as cathode exhibits lower polarization resistance and ohmic resistance than those of a cell-B at 700 °C. The results show that the introduction of YDB to an anode-supported SOFC with a LSGM/LDC composite electrolyte film can effectively block electronic transport through the cell and thus increased the OCVs, and can help the cell to achieve higher power output.

1. Introduction

Strontium- and magnesium-doped lanthanum gallate (LSGM) perovskite-type compounds are considered as promising solid electrolytes for intermediate-temperature solid oxide fuel cell (IT-SOFC) applications. Both the high conductivity of LSGM materials and the expected high performance continue to stimulate research on LSGM thin-film cells [1,2]. Recently, many efforts have been made to fabricate SOFC single cells with LSGM thin electrolyte films [3,4]. However, the preparation of anode-supported LSGM thin films by the co-firing technique appears to be difficult due to the serious reactions between LSGM and the traditionally used anode catalyst Ni at high temperatures. The chemical reactions at high temperatures between the LSGM and NiO can be avoided in an iso-La chemical activity cell [5,6]. A better choice for these IT-SOFCs is to use lanthanum-doped ceria (LDC) as an interlayer between the LSGM electrolyte and Ni-containing anode, which can effectively restrain the reaction of LSGM and NiO. There are some previous works [5,7,8] considering LDC/LSGM/LDC trilayer electrolytes using also a LDC buffer layer to avoid reactivity between cathode and LSGM electrolyte. In these works, the LDC layers were effective in minimizing interdiffusion and reaction [7,8]. On the other hand, the open-circuit voltages (OCVs) of the cells based on LDC/LSGM/LDC trilayer as reported in their previous work were lower than the theoretical electromotive force, which could be due to electronic conductivity in the LSGM layer. Moreover, by increasing the ionic conductivity of the materials used as an interlayer in the composite electrolyte, it is possible to lower the total electrolyte resistance.

Doped bismuth oxides have an ionic conductivity one order of magnitude higher than that of LDC at comparable temperatures. They are pure oxide conductors and are kinetically stable under oxygen partial pressures above 10^{-13} atm at about 600 °C [9–12]. In the absence of contact with an active reducing agent (such as H_2), doped bismuth oxide, such as erbia-stabilized bismuth oxide (ESB), has been used to block the electron penetration of doped ceria [12,13]. Moreover, due to the higher ionic conductivity of doped bismuth oxide compared to that of doped ceria, higher electrical conductivity of a bilayered doped bismuth oxide and doped ceria composite electrolyte can be expected compared to that of a singly doped ceria electrolyte [13–15]. For example, Leng et al. adopted a cost-effective wet ceramic process/painting/screen-printing method to successfully fabricate a YDB film (of thickness ~16 μm) on gadolinia-doped ceria (GDC) substrates and found that such a YDB film was effective in blocking electronic penetration through the GDC electrolyte [15]. Therefore the investigation of a new YDB/LSGM/LDC trilayer is very interesting, because YDB layer can block the electron penetration of LSGM induced by diffusion

* Corresponding author .Tel.: +86 20 2223 6168; fax: +86 20 2223 6168.
E-mail addresses: guoweimin8@163.com, guoweiminscut@163.com (W. Guo), jiangliu@scut.edu.cn (J. Liu).

0378-7753/$ – see front matter © 2010 Elsevier B.V. All rights reserved.
doi:10.1016/j.jpowsour.2010.07.039

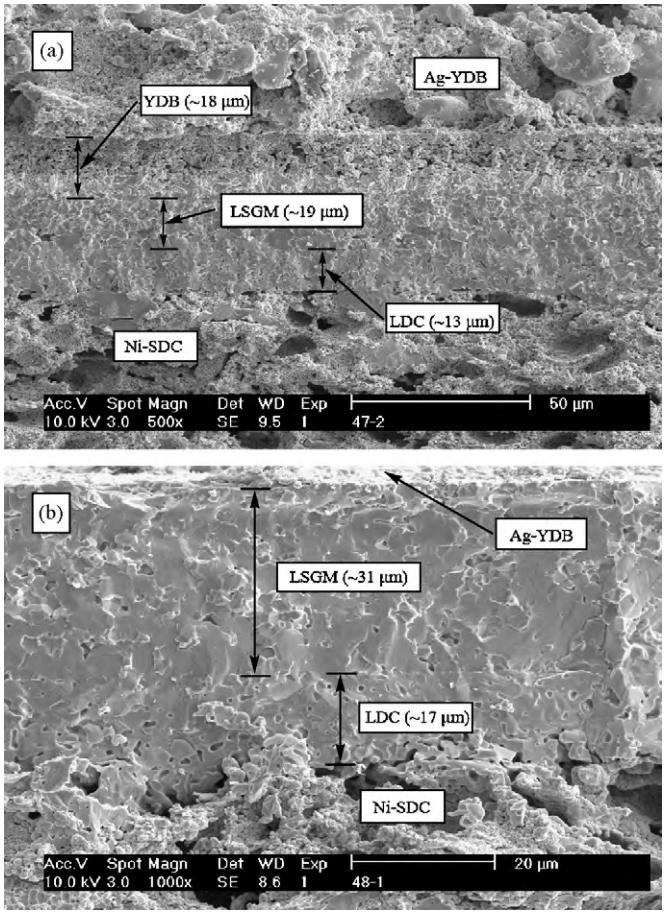

Fig. 1. SEM images of cross-sectional views of (a) cell-A with a YBD/LSGM/LDC composite electrolyte and (b) cell-B with a LSGM/LDC composite electrolyte.

of Ni during high temperature co-firing process and it has been reported an increase of the OCVs using doped bismuth/doped ceria bilayers such as ESB/GDC, YDB/YSZ and YDB/GDC.

As mentioned above, bilayer electrolytes have been commonly introduced to prevent the decomposition of doped bismuth oxide in low partial pressures of oxygen. In order to apply YDB electrolyte to a LSGM electrolyte layer as an interlayer for IT-SOFCs, we have designed trilayer electrolyte composed of a YDB layer on the oxidizing side and a LSGM/LDC composite layer on the reducing side. The advantage of this design is that LSGM, LDC, and YDB are all sufficiently conductive to serve as IT-SOFC electrolytes. In addition, compared with our previous work, YDB applied onto the LSGM electrolyte is fabricated by centrifugal casting technique as an interlayer, which may also effectively improve the electrochemical performance of the resulting trilayer electrolyte SOFCs [7,8,16,17].

In the present work, a YDB interlayer has been employed in the fabrication of anode-supported SOFCs with a LSGM electrolyte layer. To the best of our knowledge, there has not hitherto been any report on the application of a YDB/LSGM/LDC composite electrolyte in an anode-supported SOFC in the literature.

2. Experimental

$La_{0.9}Sr_{0.1}Ga_{0.8}Mg_{0.2}O_{3-\delta}$ (LSGM) and $La_{0.4}Ce_{0.6}O_{1.8}$ (LDC) powders were synthesized by conventional solid-state reactions process [7]. $Y_{0.25}Bi_{0.75}O_{1.5}$ (YDB) was prepared by reverse-titration chemical co-precipitation method [18]. The precipitate was oven-dried at 80 °C and calcined at 750 °C for 2 h to form YDB powder. $Sm_{0.2}Ce_{0.8}O_{1.9}$ (SDC) powder was prepared using a citric-nitrate process [19], and nickel oxide (NiO) powder was obtained by the precipitation method [7]. The NiO-SDC anode substrates were prepared by a conventional ceramic process as described in our previous work [7]. LSGM/LDC bilayer electrolytes were fabricated by a centrifugal casting technique. In this way, layers of first LDC and then LSGM were sequentially deposited on the NiO-SDC anode substrates [7,20]. The thicknesses of the LSGM and LDC layers were controlled by the amount of slurry. The deposited pellets were co-fired at 1400 °C for 4 h. A YDB layer was also fabricated on the LSGM/LDC by a centrifugal casting technique. The anode substrates with the YDB/LSGM/LDC trilayer were then sintered at 900 °C for 2 h. Before application of the cathodes, the gas tightness of as-fired samples was characterized with a vacuum measurement apparatus as described by previously Barnett el at. [21]. The porous cathode was prepared using a mixture of Ag and YDB in a weight ratio of 6:4 with an ethylcellulose–terpineol vehicle [22]. The mixture was applied to the electrolyte and then fired at 750 °C for 1 h in air. The as-fabricated SOFCs with the YDB/LSGM/LDC and LSGM/LDC composite electrolytes are designated as cell-A and cell-B, respectively.

A single cell was assembled by attaching a cell pellet to one end of an alumina tube using silver paste as a sealant and joint material. The cells were tested with an electrochemical instrument (Autolab PGSTAT30, Holland). Hydrogen was passed over the anode at a flow rate of 75 mL min^{-1}, while the cathode was exposed to ambient air. After reducing the NiO-containing anode at 500 °C in H_2 for several hours, the performance of the cell was tested from 500 to 700 °C. The morphology and microstructure of the single cells were characterized with a Philips XL-30FEG scanning electron microscope (SEM). AC impedance spectroscopy was typically carried out in the frequency range from 0.01 Hz to 100 kHz with a signal amplitude of 20 mV under open-circuit conditions at temperatures between 500 and 700 °C.

3. Results and discussion

XRD analysis showed the as-prepared LSGM powder and YDB powder to be in good agreement with the diffraction data for a perovskite phase and expected peaks for a δ-Bi_2O_3 phase with no indication of any second phase, respectively.

Fig. 1 shows SEM images of cross-sectional views of cell-A (Fig. 1a) and cell-B (Fig. 2b). The total thickness of the YDB/LSGM/LDC composite electrolyte film was 50 μm (18 μm YDB + 19 μm LSGM + 13 μm LDC). The thickness of the LSGM/LDC film was controlled to be almost the same at 48 μm (31 μm LSGM + 17 μm LDC). As can be seen from the SEM images, the YDB, LSGM and LDC trilayers were sintered well together with good intimate contact and surrounding electrodes. The LSGM and LDC layers were relatively dense, and the location of YDB layer closed to LSGM layer was tight while the location away from LSGM layer was actually porous. A further increase in the sintering temperature of the YDB layer would have led to a change in its composition due to the evaporation of bismuth [15]. The obtained YDB layer with a porous microstructure still exhibited a better electrochemical performance of the cells as discussed later, although a dense YDB layer might have been better.

Fig. 2 shows open-circuit voltage (OCV) and maximum power density as a function of operating temperature for cell-A and cell-B from 500 to 700 °C (Fig. 2a) and cell voltage and power density measured at 700 °C as a function of current density for cell-A and cell-B (Fig. 2b), each with an Ag-YDB cathode. The OCV of cell-A at 700 °C was 1.006 V slightly higher than cell-B of 0.912 V, indicated that the electron penetration of LSGM induced by diffusion of Ni during high temperature co-firing process was effectively blocked by YDB/LSGM/LDC trilayers. In comparison with our pre-

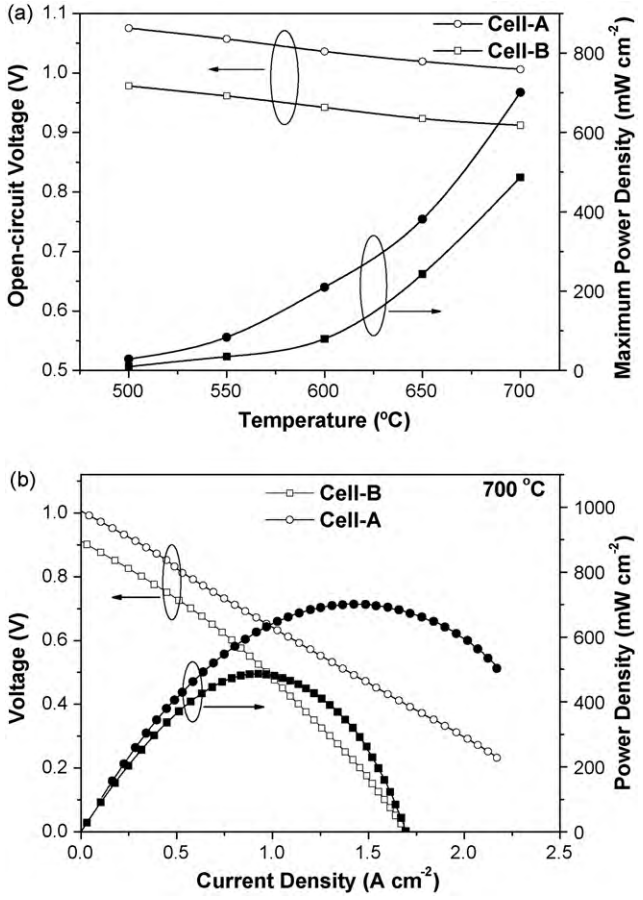

Fig. 2. (a) OCV and maximum power density as a function of operating temperature and (b) cell voltage and power density measured at 700 °C as a function of current density for cell-A and cell-B.

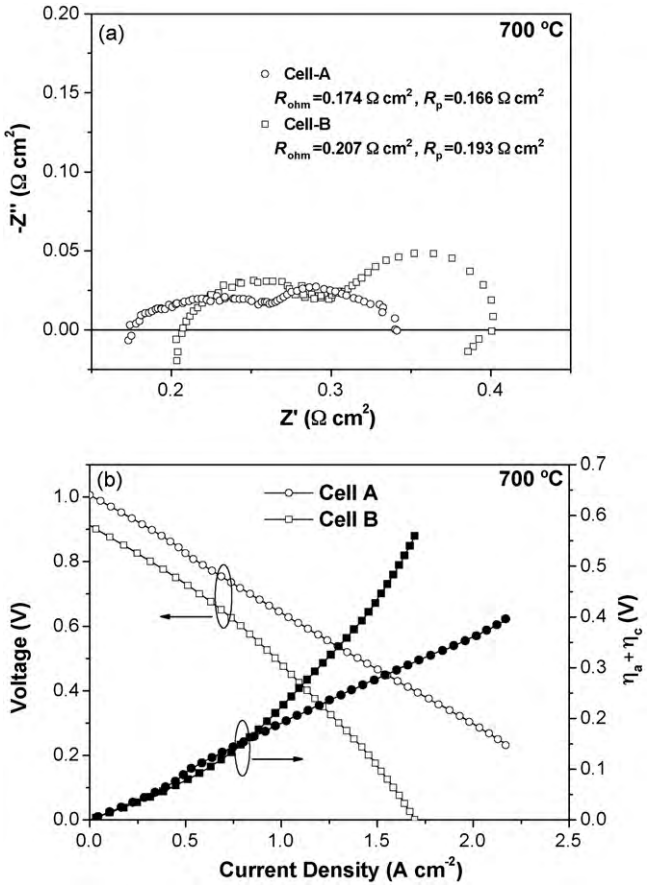

Fig. 3. (a) Impedance spectra measured under open-circuit conditions and cell voltage and (b) electrode polarization loss as a function of current density for cell-A and cell-B at 700 °C.

vious work [7,23], the slight increase of the OCV value may be due to the use of a YDB layer. Correspondingly, the maximum power density was 701 mW cm^{-2}, which is 44% higher than that of cell-B (i.e., 487 mW cm^{-2}). The improvement in cell performance of cell-A is believed to be due to the combined effect of its lower polarization resistance of oxygen reduction at the Ag-YDB/YDB interface and lower ohmic resistance. Cell-A showed the OCVs of 1.075–1.0 V in the operating temperature range of 500–700 °C. The maximum power densities of cell-A were 701, 210, and 29 mW cm^{-2} at 700, 600, and 500 °C, respectively, these values being higher than those for cell-B at the same operating temperatures (i.e., 487, 80, and 7 mW cm^{-2}, respectively).

Fig. 3 shows impedance spectra and cell voltage (Fig. 3a) and electrode polarization loss as a function of current density (Fig. 3b) for cell-A and cell-B at 700 °C, each with an Ag-YDB cathode. The cells were measured at 700 °C. The respective ohmic resistances and electrode polarization resistances were evaluated from the impedance spectra. The measured specific ohmic resistance of cell-A evaluated from the impedance spectrum was 0.174 Ω cm^2 at 700 °C, which was observably higher than the calculated value 0.0663 Ω cm^2 based on prior reported bulk electrolytes conductivity in literatures [24–26]. The measured specific ohmic resistance across the LSGM/LDC two-layer electrolyte film was 0.207 Ω cm^2 higher than that of cell-B of 0.0824 Ω cm^2 at 700 °C. This is likely because the bulk conductivity of LDC in a single cell under operating condition is higher than that measured directly on the electrolyte under air atmosphere [27], and the contribution to the ohmic resistance of the electrodes or possible interfacial reactions between the cell components will be convinced in the next study. The result suggested that under fuel cell operating conditions, the total conductivity of the YDB/LSGM/LDC composite electrolyte was higher than that of the LSGM/LDC composite electrolyte. The polarization resistance of cell-A was 0.166 Ω cm^2, which was about 50% of the total resistance and was 14% lower than that of cell-B of 0.193 Ω cm^2. Because the anodes of the two cells were the same, it was believed that the interfacial resistance of oxygen reduction at the Ag-YDB/YDB interface was slightly lower than that at the Ag-YDB/LSGM interface. The electrode polarization is calculated by means of the following equation:

$$\eta_a + \eta_c = \mathrm{OCV} - iR_{\mathrm{ohm}} - E$$

where η_a is the anode polarization loss, η_c is the cathode polarization loss, OCV is the open-circuit voltage, R_{ohm} is the ohmic resistance obtained from the impedance plot in Fig. 3a, and E is the cell voltage at current density i. The polarization loss for cell-A was found to be much lower than that of cell-B at higher current density of 1.19 A cm^{-2}. Because Ni-SDC anode polarization resistance/loss is normally much smaller than Ag-YDB cathode polarization resistance/loss, the cathode polarization loss at the Ag-YDB/YDB interface was lower than that at the Ag-YDB/LSGM interface. Another conclusion from Fig. 2 is that the good performance of cell-A, compared to thin-YSZ electrolyte cells, was attributed primarily to the reduced ohmic resistance of the trilayer electrolyte.

In this study, the total thickness of the YDB/LSGM/LDC composite electrolyte was 50 μm, the cathode was Ag-YDB, and the YDB layer was not fully dense (Fig. 1a). Leng et al. [15] have reported that the power density may have been significantly improved

using a thinner composite electrolyte with a denser YDB layer and adopting a more active material as the cathode. Furthermore, Ag-containing cathodes such as Ag-$(BaO)_{0.11}(Bi_2O_3)_{0.89}$ [28] or Ag-bismuth oxide [29,30] and Ag-BICUVOX.10 [31] cathodes based on perovskite-based materials such as $La_{0.7}Sr_{0.3}CoO_{3-\delta}$ cathode [32], and bismuth-ruthenate-based cathodes such as $Bi_2Ru_2O_7$ [33] may be used in SOFCs with the YDB/LSGM/LDC composite electrolyte.

4. Conclusions

A YDB interlayer has been deposited on a LSGM/LDC composite electrolyte using a centrifugal casting technique. In this way, anode-supported SOFCs with a trilayered YDB/LSGM/LDC composite electrolyte film have been developed. A cell consisting of a YDB/LSGM/LDC composite electrolyte film showed a slight improvement in maximum power density compared with the corresponding values and a slight reduction in polarization loss at the electrolyte/cathode interface for a cell consisting of a LSGM/LDC composite electrolyte film. The YDB layer has effectively blocked electronic transport through the cell and thus increased the OCVs. As a result, the introduction of YDB to an anode-supported SOFC with a LSGM/LDC composite electrolyte film will help the cell to achieve higher power output. Therefore, the results suggest the potential application of the YDB/LSGM/LDC composite as a promising electrolyte for IT-SOFCs.

Acknowledgements

The authors gratefully acknowledge financial support from the National High Technology Research Development Project of China (No. 2007AA05Z136), the Key Project of Ministry of Education of China (No. 210163), the Natural Science Foundation of Guangxi Zhuang Autonomous Region (No. 2010GXNSFA013045), the Department of Education of Guangxi Autonomous Region (No. 200911MS113) and Guangxi University of Technology (No. 09304).

References

[1] T. Ishihara, H. Matsuda, Y. Takita, J. Am. Chem. Soc. 116 (1994) 3801–3803.
[2] J.H. Wan, J.Q. Yan, J.B. Goodenough, J. Electrochem. Soc. 152 (2005) A1511–A1515.
[3] J.W. Yan, Z.G. Lu, Y. Jiang, Y.L. Dong, C.Y. Yu, W.Z. Li, J. Electrochem. Soc. 149 (2002) A1132–A1135.
[4] Z.H. Bi, B.L. Yi, Z.W. Wang, Y.L. Dong, H.J. Wu, Y.C. She, M.J. Cheng, Electrochem. Solid-State Lett. 7 (2004) A105–A107.
[5] K.Q. Huang, J.H. Wan, J.B. Goodenough, J. Electrochem. Soc. 148 (2001) A788–A794.
[6] Y. Matsuzaki, I. Yasuda, Solid State Ionics 152–153 (2002) 463–468.
[7] W.M. Guo, J. Liu, Y.H. Zhang, Electrochim. Acta 53 (2008) 4420–4427.
[8] Y.B. Lin, S.A. Barnett, Electrochem. Solid-State Lett. 9 (2006) A285–A288.
[9] N.M. Sammes, G.A. Tompsett, H. Näfe, F. Aldinger, J. Eur. Ceram. Soc. 19 (1999) 1801–1826.
[10] P. Shuk, H.D. Wiemhöfer, U. Guth, W. Göpel, M. Greenblatt, Solid State Ionics 89 (1996) 179–196.
[11] K.Z. Fung, H.D. Baek, A.V. Virkar, Solid State Ionics 52 (1992) 99–104.
[12] E.D. Wachsman, P. Jayaweera, N. Jiang, D.M. Lowe, B.G. Pound, J. Electrochem. Soc. 144 (1997) 233–236.
[13] J.Y. Park, H. Yoon, E.D. Wachsman, J. Am. Ceram. Soc. 88 (2005) 2402–2408.
[14] S.H. Chan, X.J. Chen, K.A. Khor, Solid State Ionics 158 (2003) 29–43.
[15] Y.J. Leng, S.H. Chan, Electrochem. Solid-State Lett. 9 (2006) A56–A59.
[16] T. Ishihara, T. Shibayama, M. Honda, H. Nishiguchi, Y. Takita, Chem. Commun. (1999) 1227–1228.
[17] T. Ishihara, T. Shibayama, H. Nishiguchi, Y. Takita, J. Mater. Sci. 36 (2001) 1125–1131.
[18] Q. Zhen, G.M. Kale, G. Shi, R. Li, W.M. He, J.Q. Liu, Solid State Ionics 176 (2005) 2727–2733.
[19] D.H.A. Blank, H. Kruidhof, J. Flokstra, J. Phys. D: Appl. Phys. 21 (1988) 226–227.
[20] J. Liu, S.A. Barnett, J. Am. Ceram. Soc. 85 (2002) 3096–3098.
[21] P.V. Dollen, S.A. Barnett, J. Am. Ceram. Soc. 88 (2005) 3361–3368.
[22] C.R. Xia, Zhang, M.L. Liu, Appl. Phys. Lett. 82 (2003) 901–903.
[23] W.M. Guo, J. Liu, C. Jin, H.B. Gao, Y.H. Zhang, J. Alloys Compd. 473 (2009) 43–47.
[24] D. Singman, J. Electrochem. Soc. 113 (1966) 502–504.
[25] C.B. Choudhary, H.S. Maiti, E.C. Subbarao, Solid Electrolytes and Their Applications, first ed., Plenum Press, New York, 1980, pp. 40.
[26] T. Shimonosono, Y. Hirata, S. Sameshima, J. Am. Ceram. Soc. 88 (2005) 2114–2120.
[27] Z.H. Bi, Y.L. Dong, M.J. Cheng, B.L. Yi, J. Power Sources 161 (2006) 34–39.
[28] S.G. Huang, Z. Zong, C.Q. Peng, J. Power Sources 173 (2007) 415–419.
[29] M. Camaratta, E. Wachsman, Solid State Ionics 178 (2007) 1242–1247.
[30] M. Camaratta, E. Wachsman, Solid State Ionics 178 (2007) 1411–1418.
[31] C.R. Xia, M.L. Liu, Adv. Mater. 14 (2002) 521–523.
[32] V.V. Kharton, E.N. Naumovich, V.Y. Samokhval, Solid State Ionics 99 (1997) 269–280.
[33] A. Jaiswal, E.D. Wachsman, J. Electrochem. Soc. 152 (2005) A787–A790.